Tunable depletion potentials driven by shape variation of surfactant micelles

Matthew D. Gratale, Tim Still, Caitlin Matyas, Zoey S. Davidson, Samuel Lobel, Peter J. Collings, and A. G. Yodh

Phys. Rev. E **93**, 050601 — Published 11 May 2016

DOI: 10.1103/PhysRevE.93.050601

Tunable depletion potentials driven by shape variation of surfactant micelles

Matthew D. Gratale,[1] Tim Still,[1] Caitlin Matyas,[1,2] Zoey S. Davidson,[1] Samuel Lobel,[1] Peter J. Collings,[1,3] and A. G. Yodh[1]

[1] *Department of Physics and Astronomy, University of Pennsylvania, Philadelphia, PA 19104, USA*
[2] *The Arts Academy at Benjamin Rush, Philadelphia, PA 19154, USA*
[3] *Department of Physics and Astronomy, Swarthmore College, Swarthmore, PA 19081, USA*

Depletion interaction potentials between micron-size colloidal particles are induced by nanometer-scale surfactant micelles composed of hexaethylene glycol monododecyl ether ($C_{12}E_6$) and are measured by video microscopy. The strength and range of the depletion interaction is revealed to arise from variations in shape anisotropy of the surfactant micelles. This shape anisotropy increases with increasing sample temperature. By fitting the colloidal interaction potentials to theoretical models, we extract micelle length and shape anisotropy as a function of temperature. The work introduces shape anisotropy tuning as a means to control interparticle interactions in colloidal suspensions, and it shows how the interparticle depletion potentials of micron-scale objects can be employed to probe the shape and size of surrounding macromolecules at the nano-scale.

PACS numbers: 82.70.Dd,82.70.Uv,05.40.-a,61.20.-p

A well-known attraction arises between large colloidal particles when many small non-adsorbing particles, called depletants, are added to the suspension. This attractive force is entropic in origin and is often called the depletion force [1, 2]. Over the years, depletion forces have proved valuable as a means to control and study phase behavior [3–18], to direct self-assembly [19–32], and to control the stability of colloidal suspensions [33–44]. Depletion forces are also used in applications such as formulation and processing of food [45–48] and paint [49], and related entropic effects called macromolecular crowding play a role in cell biology [50, 51]. Thus it remains important to fully understand depletion phenomena and to continue to explore new means to induce and manipulate depletion forces.

Most depletants are spherical, but sometimes depletants with other geometric shapes are utilized, *e.g.,* rods or disks [33, 34, 52–65]. Depletant geometry is important. The functional form and strength of the entropic potential depends on depletant shape. At the same volume fraction, for example, small rods of length L will induce a stronger attraction than small spheres with diameter L [52–54], and the spatial form of the potential induced by rods has more curvature than that of spheres. In practice it is often desirable to vary interaction strength, and this task is usually accomplished by varying depletant volume fraction, *e.g.,* by adding or subtracting small particles [3, 7–14, 19, 29, 30, 33, 35] or by changing sphere radius [15–17, 22–24, 32]. Temperature changes in suspensions of micelles of some nonionic surfactants can also alter the depletion interaction between colloidal particles [66, 67].

In this work we introduce shape *anisotropy* tuning as a means to control depletion interactions in suspension. Specifically, we employ temperature variation to change the shape of nanometer-size surfactant micelles from sphere-like to cylinder-like. As a result, the corresponding depletion potential depth and range are modulated. The potentials are derived from video microscopy measurements of the pair correlation function of micron-sized silica spheres suspended in a solution of hexaethylene glycol monododecyl ether ($C_{12}E_6$) surfactant micelles. The depletion potentials are revealed to vary substantially in magnitude and range with temperature. We demonstrate that these effects arise from shape anisotropy variation, wherein nearly spherical $C_{12}E_6$ micelles at low temperatures evolve into cylindrical micelles of varying length at higher temperatures. By fitting the measured interaction potentials to theoretical models for depletion forces of rod-like/ellipsoidal depletants [57], we extract the length and shape anisotropy of the micelle as a function of temperature. The resultant derived dimensions of suspended micelles are found to be roughly consistent with neutron scattering data for $C_{12}E_6$ [68].

To our knowledge this contribution is the first to demonstrate temperature tuning of shape anisotropy as a means to modulate depletion interactions. Savage and Dinsmore previously employed $C_{12}E_6$ micelles to control colloid attraction as a function of temperature [4, 5]. However, since the origin of attraction was not important for their sublimation and crystallization experiments, they used the attraction effect empirically [4, 5]. Here we show explicitly that temperature-dependent variation of the attractive interaction is due to a change in shape anisotropy of surfactant micelles. Significantly, we also introduce depletion interaction measurements of micron-scale objects as a new method to extract information about the size and shape of surrounding macromolecules at the nano-scale.

To understand these phenomena we briefly recall theoretical forms of the entropic potential due to spherical, thin-rod, and ellipsoidal depletants. The well-known entropic interaction potential, $U(r)$, for spherical depletants is $U(r)/k_BT = -3\phi(R/L)\left(1-(r-2R)/L\right)^2$ [1, 2]. Here, L denotes depletant sphere diameter; k_B is the Boltzmann constant, T is temperature, ϕ is the depletant volume fraction, r is the center-to-center distance between colloidal particles, R is the large particle radius, and $r-2R$ is the surface-to-surface distance between col-

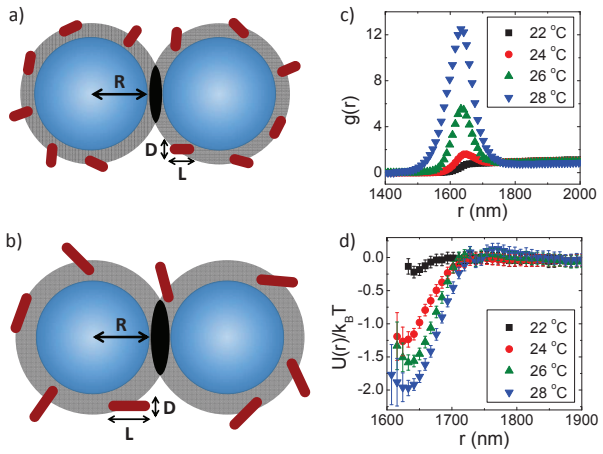

FIG. 1. Depletion between colloidal particles of radius, R, in suspension of rods with length, L, and cross-sectional diameter, D. The rod centers cannot fit within regions of excluded volume (grey shaded region). a) When excluded volumes of two spheres overlap, the rod entropy increases in proportion to excluded volume overlap (black region), and an attractive force thus arises between colloidal particles. b) When rod length, L, is increased, while keeping rod volume fraction ϕ and cross-sectional diameter D constant, then the excluded volume overlap increases, and the strength and range of the attraction between colloidal particles increases. Rods and colloidal particles not drawn to scale. c) Measured radial distribution function, $g(r)$, for temperatures 22 °C, 24 °C, 26 °C, and 28 °C. d) Measured interaction potential, $U(r)$, for temperatures 22 °C, 24 °C, 26 °C, and 28 °C.

loidal particles, sometimes denoted as h in other studies [52–54, 57]. Notice, the potential minimum (attraction strength) between particles at contact ($r = 2R$) depends on depletant volume fraction and the ratio of large- to small-sphere diameter, *i.e.*, $U(2R)/k_BT = -3\phi(R/L)$.

For thin-rod depletants, the entropic interaction is $U(r)/k_BT = -(2/3)\phi(RL/D^2)\,(1-(r-2R)/L)^3$ [52–54]. Here L is the depletant rod length, and D is the depletant rod cross-sectional width with $D/L << 1$. In this case, the potential minimum at contact remains directly proportional to the depletant volume fraction, but also depends on rod length, *i.e.*, $U(2R)/k_BT = -(2/3)\phi(RL/D^2)$. Notice that increasing rod length, while holding the rod volume fraction and cross-sectional width fixed, increases the attraction strength and decreases the number of rods. This increase in attraction strength with increasing rod length arises from a comparative increase in the free volume accessible to the longer rods, see Figures 1a and b.

When rod cross-sectional width is no longer negligible compared to rod length, the situation becomes more complex. In this case the depletants are better modeled as ellipsoids or cylinders. For ellipsoidal depletants the potential minimum is proportional to depletant volume fraction, and the long/major ellipsoid axis length (L). The aspect ratio of the ellipsoidal depletants is significant, because the attraction strength grows with increasing aspect ratio, and because the shape of the potential also depends on aspect ratio. The potential function for ellipsoidal depletants has been derived [57] and is given below; it has different functional forms for interparticle separations less than versus greater than the short/minor axis length (D). The entropic interaction is:

$$\frac{U(r;L,D,R,\phi)}{k_BT} = \phi\frac{RL}{D^2}Q(r;L,D) \tag{1}$$

with

$$Q(r;L,D) = \begin{cases} x(r) - \frac{x(r)^2}{2} - \frac{2}{3} - \frac{4}{3}A^{-2} + \frac{x(r)}{A\sqrt{A^2-1}}\ln\left(A+\sqrt{A^2-1}\right) & 2R \le r < 2R+D \\ x(r) - \frac{x(r)^2}{2} - \frac{2}{3} - \frac{4}{3}A^{-2} + \frac{\left[(Ax(r))^2+8\right]\sqrt{(Ax(r))^2-4}}{12A^2\sqrt{A^2-1}} & \\ \quad + \frac{x(r)}{A\sqrt{A^2-1}}\ln\left(2\frac{A+\sqrt{A^2-1}}{Ax(r)+\sqrt{(Ax(r))^2-4}}\right) & 2R+D \le r < 2R+L, \end{cases} \tag{2}$$

where $x(r) = (r-2R)/(L/2)$ is the dimensionless interparticle separation, and $A = L/D$ is the ellipsoid aspect ratio. We employ this functional form of the interparticle potential for fitting to data.

To experimentally measure the shape-dependent depletion interaction induced by $C_{12}E_6$ micelles, we suspend 1625 nm diameter silica microspheres (Duke Scientific) with 30 nm size standard deviation in a solution of 44 mM $C_{12}E_6$ and 17 mM NaCl. The critical micelle concentration (CMC) of $C_{12}E_6$ is 7.2×10^{-2} mM at 25 °C [69]. Thus, the concentration of surfactant is more than 600 times that of the CMC; therefore, small changes in CMC with temperature should not significantly affect the suspended micelles. Specifically, as the sample temperature changes, we expect the micelle volume fraction to remain constant. As a result, the depletant volume fraction was held constant in fits at all temperatures and was set equal to the volume fraction of surfactant in water, *i.e.*, $\phi = 0.02$.

The Debye screening length κ^{-1} in water is calculated using $\kappa^{-1} = 0.304/\sqrt{I(M)}$, where $I(M)$ is ionic strength expressed in molar concentration (mol/L) [70]. The salt

concentration, $I(M) = 0.017$ mol/L, yields a screening length $\kappa^{-1} = 2.3$ nm. Although this screening length is negligible compared to the colloidal particle diameter, it is significant when compared to the micelle length and width [68]. At first glance, it might be expected that micelle of the nonionic surfactant, $C_{12}E_6$, should be assigned a net charge of zero. In this case, the screening length should be ignored, and the "bare" rod length, L, and rod width, D, should be used in the depletion potential analysis. However, considerable evidence exists to support the notion that ethylene oxide groups of the $C_{12}E_6$ surfactant micelles can acquire charge in the presence of salt [71–73]. In this case, dressed dimensions that incorporate the screening length should be used in the analysis. Because of this debate, we carry out two sets of calculations: using the "bare" dimensions, L and D, and using dressed dimensions. For the calculations preformed with the "dressed" dimensions, we introduce an *effective* rod length, $L' = L + 2\kappa^{-1}$, and an *effective* rod width, $D' = D + 2\kappa^{-1}$, in place of L and D in Equation 1; with this notation, L and D are the "true", or "bare", length and width of the rod, respectively.

Samples were prepared by loading particle-surfactant solution between two glass coverslips. The concentration of silica spheres was selected such that the areal packing density, ρ, was approximately 0.08 in the two-dimensional (2D) regions we studied. The temperature of the sample was controlled via an objective heater (Bioptechs), and measurements were made for temperatures ranging from 22 °C to 28 °C in 1 °C steps. Bright-field microscopy video was recorded at 30 frames per second for $65,000$ frames. Subpixel particle tracking algorithms were employed to find particle positions in each frame of the video [74].

Previous small angle neutron scattering (SANS) experiments provide independent estimates about the shape of $C_{12}E_6$ micelles. In this work, the micelles were modeled as a monodisperse distribution of rod-like cylinders with spherical caps. With increasing temperature, the length of the rods was measured to increase, while the cross-sectional diameter remained constant. Specifically, the length increases from approximately $19 - 31$ nm over the temperature range studied in our work, and the cross-sectional diameter remains constant at approximately 4.3 nm [68]. Since, the aspect ratio ranges between 4.4 and 7.2, and since the cross-sectional diameter of the micelles is not negligible, it is critical to employ the more complex functional form (Eq.1) as a theoretical model for the interaction potential [57].

In our experiments, the sample radial distribution function, $g(r)$, was calculated using the measured particle positions. Corrections to $g(r)$ were carried out following procedures described in references [75, 76]. These corrections enable us to account for incorrect identification of particle centroids caused by overlapping of neighboring particle Airy disks. Exemplary $g(r)$ curves, after the Airy disk correction, are given in Fig. 1c.

The pair interaction potential $U(r)$ is derived from the radial distribution function $g(r)$. Briefly, in the limit where particle areal packing density ρ approaches zero, $g(r) = exp[-U(r)/k_bT]$. When the particle areal packing density is finite, however, as is the case in our experiment, then $g(r)$ is related to the potential of mean force, $w(r)$, via the Boltzmann relation, $g(r) = exp[-w(r)/k_BT]$ [77]. Therefore to extract the true pair interaction potential, $U(r)$, we must employ closure relations to solve the Ornstein-Zernike integral equation [77]. We utilize the Hypernetted Chain (HNC) approximation for this task. The true pair interaction potential $U(r)$ is calculated numerically from the experimentally measured $g(r)$ using the relations below:

$$\frac{U(r)}{k_BT} = \frac{w(r)}{k_BT} + \frac{\rho}{\pi R^2} I(r) \tag{3}$$

where $I(r)$ is the convolution integral,

$$I(r) = \int [g(r') - 1 - \frac{\rho}{\pi R^2} I(r)][g(|r - r'|) - 1] d^2r'. \tag{4}$$

These equations are readily solved numerically [78]. Note, we found the HNC results to be in excellent agreement with results obtained using the Percus-Yevick approximation.

Finally, to account for effects of all other interactions, *i.e.,* especially imaging artifacts not caused by depletants, the pair interaction potential between silica spheres was also measured in the absence of depletants. The zero-depletant interaction potential was then subtracted from the measured pair interaction potentials with depletants. In this way it was possible to derive pure depletion interaction potentials more accurately. At the lowest temperatures (22 °C - 24 °C), the potential well depth was small, *i.e.,* on the order of the measurement error, and full subtraction was critical. However, at higher temperatures (25 °C - 28 °C), the well depths were large and subtraction was only necessary for interparticle distances, r, larger than the range of the potential well.

To extract interaction potentials and related sample properties we implemented a straightforward but multi-step approach. The experimental data was fit assuming a theoretical potential function, $U(r)$, based on the ellipsoid model [57] (Eq.1). We first describe the procedure assuming the micelles are screened. The first step of the fitting procedure computes a theoretical potential $U_{t,i}(r; L_i', D', R, \phi)$ with an initial guess for the effective rod length L'. The other parameters, effective cross-section diameter $D' = D + 2\kappa^{-1}$, colloid radius R, and depletant volume fraction (ϕ), were tightly constrained by experiment and treated as constants; D' was set to 8.9 nm, R was set to 1625 nm, and ϕ was set to 0.02. The resulting initial estimate for the theoretical potential $U_{t,i}(r; L_i', D', R, \phi)$ was then converted into a model pair correlation function, $g_{t,i}(r)$, via the Boltzmann distribution, $g_{t,i}(r) = exp[-U_{t,i}(r; L_i', D', R, \phi)/k_BT]$.

Next, to account for the effects of colloidal particle polydispersity in the experiment, $g_{t,i}(r)$ was broadened using a Gaussian kernel for the particle size with

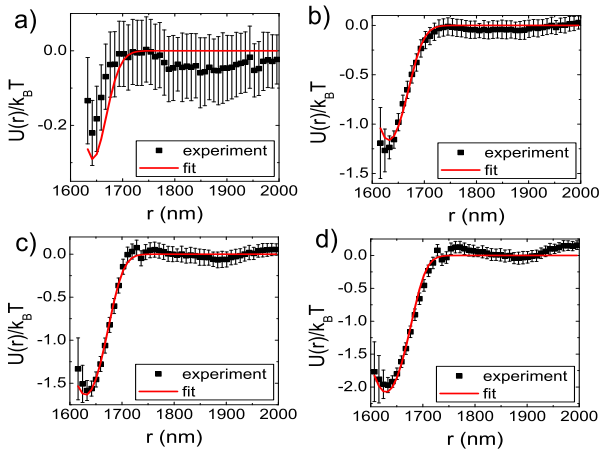

FIG. 2. Experimentally measured interparticle potentials $U(r)/k_BT$ (black squares) and fits from the theoretical function for ellipsoidal depletants (red lines) at temperatures a) 22 °C, b) 24 °C, c) 26 °C, and d) 28 °C.

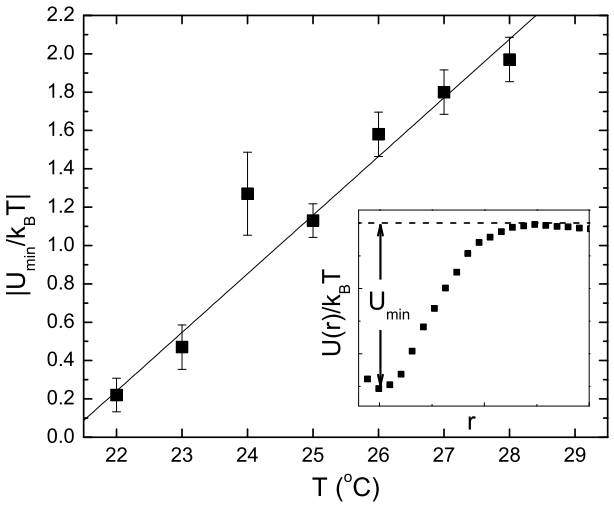

FIG. 3. Absolute value of potential minima $|U_{min}/k_BT|$ of interaction potentials versus temperature T. Inset: Sample measured interparticle potential $U(r)$ showing U_{min} represents the potential well depth.

standard deviation σ, $ker(r,\sigma) = exp[-r^2/2\sigma^2]$. The standard deviation σ was set to 30 nm and kept fixed throughout the fitting process. Convolving the theoretical pair correlation function $g_{t,i}(r)$ with the Gaussian kernel yields a broadened pair correlation function, $g^B_{t,i}(r) = [g_{t,i} * ker](r)$, which incorporates particle polydispersity. The broadened pair correlation function was then converted back to a broadened interaction potential $U^B_{t,i}(r; L'_i, D', R, \phi, \sigma)$ by taking the natural logarithm, *i.e.,* $U^B_{t,i}(r; L'_i, D', R, \phi, \sigma)/k_BT = -\ln(g^B_{t,i}(r))$.

The effective depletant length L' was extracted by least-squares fitting of the experimentally determined $U(r)$ to the polydispersity broadened theoretical interaction potential $U^B_{t,i}(r; L'_i, D', R, \phi, \sigma)$. Finally, the "true" depletant length, L, was derived by subtracting the Debye screening length factor from the best-fit effective length, *i.e.,* $L = L' - 2\kappa^{-1}$. The exact same fitting procedure was also performed assuming that the micelles were not screened in suspension; in this case we used the "bare" rod length, L, and "bare" rod width, D, in place of the effective length, L, and effective width, D, respectively. The "bare" length, L, is extracted directly from the fits.

Exemplary potentials with fits are shown in Figure 2 for the micelles with screening. It is apparent that the depth of the potential well increases monotonically with temperature. The absolute value of the minimum of the measured potential, $|U_{min}/k_BT|$, is plotted as a function of temperature in Figure 3. Note that $|U_{min}/k_BT|$ is the potential well depth, defined here as the minimum value of the potential curve $U(r)$. The potential well depth increases from $\approx 0.2k_BT$ to $\approx 2k_BT$ over the range of temperatures studied. Thus, the interparticle interaction can be tuned from nearly hard-sphere to modestly attractive by increasing sample temperature. Further, the range of the interaction grows with increasing temperature; this effect is apparent from the widths of the $g(r)$ peaks in Fig. 1c and the widths of $U(r)/k_BT$ in Fig. 1d and Fig. 2.

In addition to the monodisperse rod distributions, we also considered the case wherein the distribution of lengths of the rod-like $C_{12}E_6$ surfactant micelles is polydisperse. The polydispersity model we employ is derived from the "Ladder Model" described by Missel *et al* [79]. Here, the model and fitting procedure are briefly outlined.

Briefly, it is straightforward to show that the total micelle length, L, is directly proportional to the number of surfactant molecules that compose the micelle, N, *i.e.,* $L(N) = D + 4(N - N_0)D/\pi N_0$. Here D is the diameter of the cylindrical rods, and the number of surfactant molecules in a spherical micelle with diameter D is the minimum aggregation number, N_0. This result is derived using simple geometric arguments based on micelle shape, the shape of the individual surfactant molecule (*e.g.,* the size of the surfactants hydrophilic head group), and the packing of surfactant molecules into the micelles. We next assume that the number concentration of micelles of length $L(N)$ in solution, $X_{L(N)}$, has the exponential form [79]: $X_{L(N)} = Ce^{-N/M}$. Here C is a normalization constant in units of number concentration, and M is a constant that defines the distribution. C is derived when normalizing the distribution for the total volume fraction of micelles in solution, and M is extracted by fitting to our experimentally measured $U(r)$.

The volume fraction of micelles length $L(N)$ in solution, $\phi_{L(N)}$, is:

$$\phi_{L(N)} = X_{L(N)} D^3 \left(\frac{\pi}{6} + \frac{N - N_0}{N_0} \right). \qquad (5)$$

To derive the interaction potential induced by a poly-

disperse suspension of rod-like micelles, we simply substitute $\phi_{L(N)}$ and $L(N)$ for ϕ and L, respectively, into Equation 1, and perform the summation over N. This procedure gives:

$$\frac{U(r;M,N_0)}{k_BT} = \frac{R}{D^2}\sum_{N=N_0}^{\infty}\phi_{L(N)}L(N)Q(r;L(N),D). \quad (6)$$

The average length of the micelles, $\langle L\rangle$, is derived from an average over the concentration distribution.

Since Equation 6 is a function of M, the first step of this fitting procedure for the polydisperse rod distribution computes a theoretical potential $U_{t,i}(r;M_i,N_0,D',R,\phi)$ with an initial guess for M. D', R, and ϕ are set to the same values as before and are again treated as constant. The minimum aggregation number N_0 is set to 135 [80]. From this step forward, the same procedure described earlier is followed, and M is extracted by least-squares fitting of the experimentally determined $U(r)$. With the value of M, the distribution of micelle sizes and the average micelle length, $\langle L\rangle$, can be calculated for all temperatures. This procedure was carried out for bare and dressed micelles.

The observed increase in range and strength of the depletion attraction between colloidal particles is consistent with an increasing length of the rod-like micelle depletants. This effect is exhibited by the rod lengths L extracted from the fits. In Figure 4a, the lengths extracted from the interaction potential fits using the monodisperse model ("bare" and "dressed") are plotted as a function of temperature. In Figure 4b, the average lengths extracted from the interaction potential fits using the polyddisperse model ("bare" and "dressed") are plotted as a function of temperature. Also shown in Figures 4a and 4b are the lengths measured by small angle neutron scattering (SANS) [68]. We observe that with the monodisperse model, the lengths obtained using the "bare" dimensions in the fitting procedure are in fairly good agreement with the lengths obtained using the "dressed" dimensions and with the SANS data. Importantly, in both cases, we observe an increase in shape anisotropy of the rod-micelles with increasing temperature, which in turn leads to the increase in the strength of the depletion interaction between colloidal particles in suspension. For the polydisperse model, the average lengths obtained using both the "dressed" and "bare" dimensions in the fitting procedure are in fairly good agreement with those obtained by SANS [68]. Again, in both cases, we observe an increase in average shape anisotropy of the rod-micelles with increasing temperature. Thus, regardless of microscopic model, the nano-scale increase in shape anisotropy of $C_{12}E_6$ surfactant micelles with increasing sample temperature is apparent from measurements of the micelle-induced depletion interaction between colloidal spheres. The assignment of an exact length to the micelles (versus temperature), depends on whether the bare or dressed dimensions are used in the fits and whether the rod distributions are considered monodisperse or polydisperse. In practice, we believe the polydisperse dressed rod-micelle model is the most accurate microscopic description of this system, but here we report all other fits for the benefit of readers who might have a different opinion about micelle charge and micelle size polydispersity.

Looking forward, *in situ* modulation of colloidal attraction via shape anisotropy offers new routes for assembly of colloidal glasses and colloidal bigels [81, 82]. In contrast to most previous studies of the state diagram of colloidal glasses with attractive interparticle interactions [7–12], for example, the present system permits easy phase space exploration with the same sam-

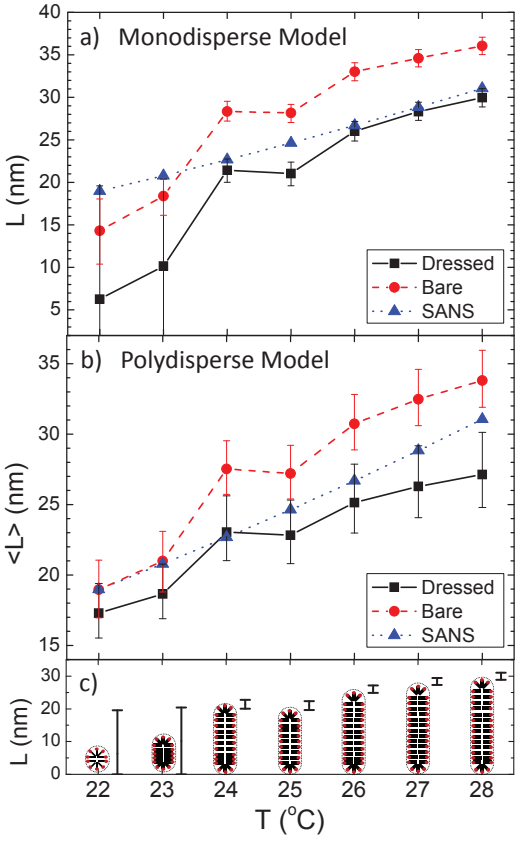

FIG. 4. a) Bare rod length L of the surfactant micelles measured by depletion interaction using the monodisperse model with "dressed" dimensions (black squares) and "bare" dimensions (red circles), and by small angle neutron scattering SANS (blue triangles) in ref. [68] versus temperature T. b) Average bare rod length $\langle L\rangle$ of the surfactant micelles measured by depletion interaction using the polydisperse model with "dressed" dimensions (black squares) and "bare" dimensions (red circles), and by small angle neutron scattering SANS (blue triangles) in ref. [68] versus temperature T. c) Cartoon representations of change in dimensions, L and D, as obtained by the "dressed" monodisperse model, of the surfactant micelles as function of temperature T. Note, D remains constant.

ple simply by changing temperature. In a different vein, the novel experimental method, along with a theoretical model for the interaction, offers a qualitatively new and effective means to extract information about the size and shape of depletant molecules at the nanoscale. Ultimately, the experimenter will generate strong evidence "for" or "against" each microscopic model from which a microscopic understanding of the local micro- and nano-environment around the particles can be deduced. One interesting new opportunity is to study depletion due to lyotropic chromonic liquid crystals [83–86] wherein the underlying plank-like macromolecules stack to produce rod-like mesogens which in turn assemble into liquid crystalline phases; the present method offers a novel way to measure the average length and length distribution of the stacks. In principle, the measurement also offers a tool to probe the size, shape, and folding of proteins.

We thank Yilong Han, Peter J. Yunker, Zexin Zhang, John C. Crocker, Piotr Habdas, Wei-Shao Wei, Kevin B. Aptowicz, Thomas Russell, Russell Composto, Daeyeon Lee, Amish Patel, Robert Riggleman, Daniel Sussman and Carl Goodrich for helpful discussions, and we gratefully acknowledge financial support from the National Science Foundation through DMR12-05463, the Penn MRSEC DMR11-20901 and its optical microscopy SEF, and NASA grant NNX08AO0G.

[1] S. Asakura and F. Oosawa, Journal of Polymer Science **33**, 183 (1958), ISSN 1542-6238.
[2] A. Vrij, Pure and Applied Chemistry **48**, 471 (1976).
[3] S. M. Ilett, A. Orrock, W. C. K. Poon, and P. N. Pusey, Phys. Rev. E **51**, 1344 (1995).
[4] J. R. Savage, D. W. Blair, A. J. Levine, R. A. Guyer, and A. D. Dinsmore, Science **314**, 795 (2006).
[5] J. R. Savage and A. D. Dinsmore, Phys. Rev. Lett. **102**, 198302 (2009).
[6] A. Stradner, H. Sedgwick, F. Cardinaux, W. C. K. Poon, S. U. Egelhaaf, and P. Schurtenberger, Nature **432**, 492 (2004), ISSN 0028-0836.
[7] K. N. Pham, S. U. Egelhaaf, P. N. Pusey, and W. C. K. Poon, Phys. Rev. E **69**, 011503 (2004).
[8] N. Koumakis and G. Petekidis, Soft Matter **7**, 2456 (2011).
[9] L. J. Kaufman and D. A. Weitz, The Journal of Chemical Physics **125**, 074716 (2006).
[10] A. Latka, Y. Han, A. M. Alsayed, A. B. Schofield, A. G. Yodh, and P. Habdas, EPL (Europhysics Letters) **86**, 58001 (2009).
[11] N. B. Simeonova, R. P. A. Dullens, D. G. A. L. Aarts, V. W. A. de Villeneuve, H. N. W. Lekkerkerker, and W. K. Kegel, Phys. Rev. E **73**, 041401 (2006).
[12] C. K. Mishra, A. Rangarajan, and R. Ganapathy, Phys. Rev. Lett. **110**, 188301 (2013).
[13] M. Adams, Z. Dogic, S. L. Keller, and S. Fraden, Nature **393**, 349 (1998), ISSN 0028-0836.
[14] M. Adams and S. Fraden, Biophysical Journal **74**, 669 (1998), ISSN 0006-3495.
[15] R. W. Perry, G. Meng, T. G. Dimiduk, J. Fung, and V. N. Manoharan, Faraday Discuss. **159**, 211 (2012).
[16] G. E. Fernandes, D. J. Beltran-Villegas, and M. A. Bevan, Langmuir **24**, 10776 (2008).
[17] S. L. Taylor, R. Evans, and C. P. Royall, Journal of Physics: Condensed Matter **24**, 464128 (2012).
[18] G. Petekidis, L. A. Galloway, S. U. Egelhaaf, M. E. Cates, and W. C. K. Poon, Langmuir **18**, 4248 (2002).
[19] P. D. Kaplan, J. L. Rouke, A. G. Yodh, and D. J. Pine, Phys. Rev. Lett. **72**, 582 (1994).
[20] A. G. Yodh, K. Lin, J. C. Crocker, A. D. Dinsmore, R. Verma, and P. D. Kaplan, Philosophical Transactions of the Royal Society of London A: Mathematical, Physical and Engineering Sciences **359**, 921 (2001), ISSN 1364-503X.
[21] S. Sacanna, D. J. Pine, and G.-R. Yi, Soft Matter **9**, 8096 (2013).
[22] S. Sacanna, W. T. M. Irvine, P. M. Chaikin, and D. J. Pine, Nature **464**, 575 (2010), ISSN 0028-0836.
[23] L. Rossi, S. Sacanna, W. T. M. Irvine, P. M. Chaikin, D. J. Pine, and A. P. Philipse, Soft Matter **7**, 4139 (2011).
[24] G. Meng, N. Arkus, M. P. Brenner, and V. N. Manoharan, Science **327**, 560 (2010).
[25] Y. Wang, Y. Wang, X. Zheng, G.-R. Yi, S. Sacanna, D. J. Pine, and M. Weck, J. Am. Chem. Soc. **136**, 6866 (2014), ISSN 0002-7863.
[26] D. J. Kraft, R. Ni, F. Smallenburg, M. Hermes, K. Yoon, D. A. Weitz, A. van Blaaderen, J. Groenewold, M. Dijkstra, and W. K. Kegel, Proceedings of the National Academy of Sciences **109**, 10787 (2012).
[27] S. Badaire, C. Cottin-Bizonne, J. W. Woody, A. Yang, and A. D. Stroock, J. Am. Chem. Soc. **129**, 40 (2007), ISSN 0002-7863.
[28] S. Badaire, C. Cottin-Bizonne, and A. D. Stroock, Langmuir **24**, 11451 (2008), ISSN 0743-7463.
[29] K. Zhao and T. G. Mason, Phys. Rev. Lett. **101**, 148301 (2008).
[30] E. Barry and Z. Dogic, Proceedings of the National Academy of Sciences **107**, 10348 (2010).
[31] T. Gibaud, E. Barry, M. J. Zakhary, M. Henglin, A. Ward, Y. Yang, C. Berciu, R. Oldenbourg, M. F. Hagan, D. Nicastro, et al., Nature **481**, 348 (2012), ISSN 0028-0836.
[32] T. D. Edwards, Y. Yang, W. N. Everett, and M. A. Bevan, Scientific Reports **5**, 13612 (2015).
[33] G. H. Koenderink, G. A. Vliegenthart, S. G. J. M. Kluijtmans, A. van Blaaderen, A. P. Philipse, and H. N. W. Lekkerkerker, Langmuir **15**, 4693 (1999), ISSN 0743-7463.
[34] K.-H. Lin, J. C. Crocker, A. C. Zeri, and A. G. Yodh, Phys. Rev. Lett. **87**, 088301 (2001).
[35] H. de Hek and A. Vrij, Journal of Colloid and Interface Science **84**, 409 (1981), ISSN 0021-9797.
[36] R. I. Feigin and D. H. Napper, Journal of Colloid and Interface Science **74**, 567 (1980), ISSN 0021-9797.
[37] R. Tuinier, J. Rieger, and C. de Kruif, Advances in Colloid and Interface Science **103**, 1 (2003), ISSN 0001-8686.
[38] A. Sharma, S. N. Tan, and J. Y. Walz, Journal of Colloid and Interface Science **190**, 392 (1997), ISSN 0021-9797.

[39] S. Ji and J. Y. Walz, Current Opinion in Colloid & Interface Science **20**, 39 (2015), ISSN 1359-0294.

[40] E. S. Pagac, R. D. Tilton, and D. C. Prieve, Langmuir **14**, 5106 (1998), ISSN 0743-7463.

[41] P. Richetti and P. Kékicheff, Phys. Rev. Lett. **68**, 1951 (1992).

[42] J. L. Burns, Y. de Yan, G. J. Jameson, and S. Biggs, Colloids and Surfaces A: Physicochemical and Engineering Aspects **162**, 265 (2000), ISSN 0927-7757.

[43] T. D. Edwards and M. A. Bevan, Macromolecules **45**, 585 (2012), ISSN 0024-9297.

[44] R. Verma, J. C. Crocker, T. C. Lubensky, and A. G. Yodh, Macromolecules **33**, 177 (2000).

[45] J.-L. Doublier, C. Garnier, D. Renard, and C. Sanchez, Current Opinion in Colloid & Interface Science **5**, 202 (2000), ISSN 1359-0294.

[46] V. Grinberg and V. Tolstoguzov, Food Hydrocolloids **11**, 145 (1997), ISSN 0268-005X.

[47] A. Syrbe, W. Bauer, and H. Klostermeyer, International Dairy Journal **8**, 179 (1998), ISSN 0958-6946.

[48] C. de Kruif and R. Tuinier, Food Hydrocolloids **15**, 555 (2001), ISSN 0268-005X, 5th International Hydrocolloids Conference.

[49] A. Overbeek, F. Buckmann, E. Martin, P. Steenwinkel, and T. Annable, Progress in Organic Coatings **48**, 125 (2003), ISSN 0300-9440, athens 2002.

[50] S. B. Zimmerman and A. P. Minton, Annual Review of Biophysics and Biomolecular Structure **22**, 27 (1993), pMID: 7688609.

[51] A. P. Minton, Current Opinion in Structural Biology **10**, 34 (2000), ISSN 0959-440X.

[52] H. N. Lekkerkerker and R. Tuinier, *Colloids and the depletion interaction*, vol. 833 (Springer, 2011).

[53] Y. Mao, M. E. Cates, and H. N. W. Lekkerkerker, Phys. Rev. Lett. **75**, 4548 (1995).

[54] Y. Mao, M. E. Cates, and H. N. W. Lekkerkerker, The Journal of Chemical Physics **106**, 3721 (1997).

[55] Auvray, L., J. Phys. France **42**, 79 (1981).

[56] K. Yaman, C. Jeppesen, and C. M. Marques, EPL (Europhysics Letters) **42**, 221 (1998).

[57] M. Piech and J. Y. Walz, Journal of Colloid and Interface Science **232**, 86 (2000), ISSN 0021-9797.

[58] P. van der Schoot, The Journal of Chemical Physics **112**, 9132 (2000).

[59] A. W. C. Lau, K.-H. Lin, and A. G. Yodh, Phys. Rev. E **66**, 020401 (2002).

[60] R. Roth, Journal of Physics: Condensed Matter **15**, S277 (2003).

[61] L. Helden, R. Roth, G. H. Koenderink, P. Leiderer, and C. Bechinger, Phys. Rev. Lett. **90**, 048301 (2003).

[62] M. Triantafillou and R. D. Kamien, Phys. Rev. E **59**, 5621 (1999).

[63] N. Doshi, G. Cinacchi, J. S. van Duijneveldt, T. Cosgrove, S. W. Prescott, I. Grillo, J. Phipps, and D. I. Gittins, Journal of Physics: Condensed Matter **23**, 194109 (2011).

[64] L. Harnau and S. Dietrich, Phys. Rev. E **69**, 051501 (2004).

[65] D. A. Triplett and K. A. Fichthorn, The Journal of Chemical Physics **133**, 144910 (2010).

[66] S. Buzzaccaro, J. Colombo, A. Parola, and R. Piazza, Phys. Rev. Lett. **105**, 198301 (2010).

[67] R. Piazza, S. Buzzaccaro, A. Parola, and J. Colombo, Journal of Physics: Condensed Matter **23**, 194114 (2011).

[68] J. Gapinski, J. Szymanski, A. Wilk, J. Kohlbrecher, A. Patkowski, and R. Holyst, Langmuir **26**, 9304 (2010), ISSN 0743-7463.

[69] L.-J. Chen, S.-Y. Lin, C.-C. Huang, and E.-M. Chen, Colloids and Surfaces A: Physicochemical and Engineering Aspects **135**, 175 (1998), ISSN 0927-7757.

[70] J. N. Israelachvili, *Intermolecular and Surface Forces* (Academic Press, 1985), 1st ed.

[71] A. W. Wills, D. J. Michalak, P. Ercius, E. R. Rosenberg, T. Perciano, D. Ushizima, R. Runser, and B. A. Helms, Advanced Functional Materials **25**, 4120 (2015), ISSN 1616-3028.

[72] . Seung Hyun Kim, . Matthew J. Misner, . Ling Yang, . Oleg Gang, . Benjamin M. Ocko, , and . Thomas P. Russell*, Macromolecules **39**, 8473 (2006).

[73] G. S. MacGlashan, Y. G. Andreev, and P. G. Bruce, Nature **398**, 792 (1999), ISSN 0028-0836.

[74] J. C. Crocker and D. G. Grier, Journal of Colloid and Interface Science **179**, 298 (1996), ISSN 00219797.

[75] J. Baumgartl and C. Bechinger, EPL (Europhysics Letters) **71**, 487 (2005).

[76] M. Polin, D. G. Grier, and Y. Han, Phys. Rev. E **76**, 041406 (2007).

[77] J.-P. Hansen and I. R. McDonald, *Theory of Simple Liquids, 2nd* (Academic Press, 1986).

[78] E. M. Chan, Journal of Physics C: Solid State Physics **10**, 3477 (1977).

[79] P. J. Missel, N. A. Mazer, G. B. Benedek, C. Y. Young, and M. C. Carey, The Journal of Physical Chemistry **84**, 1044 (1980).

[80] H. G. Thomas, A. Lomakin, D. Blankschtein, and G. B. Benedek, Langmuir **13**, 209 (1997).

[81] F. Varrato, L. Di Michele, M. Belushkin, N. Dorsaz, S. H. Nathan, E. Eiser, and G. Foffi, Proceedings of the National Academy of Sciences **109**, 19155 (2012).

[82] L. Di Michele, D. Fiocco, F. Varrato, S. Sastry, E. Eiser, and G. Foffi, Soft Matter **10**, 3633 (2014).

[83] V. R. Horowitz, L. A. Janowitz, A. L. Modic, P. A. Heiney, and P. J. Collings, Phys. Rev. E **72**, 041710 (2005).

[84] J. Lydon, J. Mater. Chem. **20**, 10071 (2010).

[85] J. Lydon, Current Opinion in Colloid & Interface Science **8**, 480 (2004), ISSN 1359-0294.

[86] Y. A. Nastishin, H. Liu, S. V. Shiyanovskii, O. D. Lavrentovich, A. F. Kostko, and M. A. Anisimov, Phys. Rev. E **70**, 051706 (2004).